Phenomenological crystal-field model of the magnetic and thermal properties of the Kondo-like system UCu_2Si_2

R. Troć, Z. Gajek, A. Pikul, and H. Misiorek
W. Trzebiatowski Institute of Low Temperature and Structure Research, Polish Academy of Sciences, P.O. Box 1410, 50–950 Wrocław 2, Poland

E. Colineau and F. Wastin
European Commission, Joint Research Centre, Institute for Transuranium Elements, Postfach 2340, 76125 Karlsruhe, Germany
(Received 17 April 2013; published 17 July 2013)

The transport properties described previously [Troć *et al.*, Phys. Rev. B **85**, 224434 (2012)] as well as the magnetic and thermal properties presented in this paper, observed for single-crystalline UCu_2Si_2, are discussed by assuming a *dual* (localized-itinerant) scenario. The electronic states of the localized $5f$ electrons in UCu_2Si_2 are constructed using the effective Hamiltonian known for ionic systems, allowing us to treat the Coulomb, spin-orbital, and crystal-field interactions on equal footing. The space of parameters has been restricted in the initial steps with the aid of the angular overlap model approximation. The final crystal-field parameters, obtained from the refined steps of calculations, are relatively large (in absolute values), which we attribute to the hybridization characteristic of the metallic systems on the verge of localization. The proposed crystal-field model reproduces correctly with satisfactory accuracy the magnetic and thermal properties of UCu_2Si_2 in agreement also with the transport properties reported previously. Considerable crystal-field splitting of the ground multiplet of 2760 K is responsible for a large anisotropy in the magnetic behavior, observed in the whole temperature range explored.

DOI: 10.1103/PhysRevB.88.024416 PACS number(s): 75.30.Gw, 71.70.Ch, 71.23.An

I. INTRODUCTION

UCu_2Si_2 was reported to be a ferromagnet with the Curie temperature $T_C = 103(2)$ K like UCu_2Ge_2 ($T_C = 107$ K).[1] Both these compounds crystallize in the mostly disseminate body-centered tetragonal (bct) $ThCu_2Si_2$-type structure (space group $I4/mmm$).[2] As shown by neutron diffraction experiments made on powder[1,3] and single-crystalline[4] samples, the Cu-based silicide shows some variation in a value of an ordered uranium moment oriented along the [001] direction (c axis). The latter is equal to $1.6(1)\mu_B$ (Ref. 1) or $2.0(1)\mu_B$ (Refs. 3 and 4). As shown earlier on the polycrystalline samples, some homogeneity region with respect to a Cu/Si exchange was revealed.[5] Also, the fairly large differences in the value of the ferromagnetic (FM) moment μ_f, ranging from 1.55 to $1.75\mu_B$, of U atoms in UCu_2Si_2 have been found from the low-temperature magnetization measurements on single-crystalline samples.[6,7] These differences are believed to arise from some possible deficiency of Cu atoms in this compound, while any excess in Cu content leads to a narrowing of domain walls which in turn gives rise to a strong magnetocrystalline anisotropy effect.[5] In contrast to previous results obtained on a polycrystalline sample, more recent studies performed on a single crystal of this compound, grown by the Sn-flux procedure,[7] have indicated the lack of the narrow wall domains. Moreover, these data confirmed earlier works that a FM state is stable in the whole temperature range below $T_C = 100$ K, and that there really exists an antiferromagnetic (AFM) order, but only between T_C and T_N (=106 K). A detailed neutron single-crystalline examination of this phase[4] has revealed an incommensurate longitudinal spin-density-wave state (ILSDW) with a long periodicity $\Lambda = 85.7$ Å and with nearly a sinusoidal magnetic modulation with a propagation vector $\mathbf{k} = [0, 0, \delta]$, where $\delta = 0.116$ at 101 K. In consequence, the magnetic structure contains as many as 17 layers with an in-plane sinusoidally modulated FM order. On the other hand, another single-crystalline sample of UCu_2Si_2 obtained by the Cu-flux method,[8] such as that reported in Ref. 6, has shown two AFM phases, existing either below (≈50 K) or slightly above T_C (≈96 K). The proposed earlier by the authors[8] low-temperature AFM phase, determined from the rapid fall of low-field magnetization at $T = 50$ K, follows well a picture of the isofield magnetization curves presented in Fig. 3 of Ref. 5 for the phase with the Cu excess, of the nominal composition $UCu_{2.2}Si_{1.8}$, measured in the whole temperature region of its ferromagnetic behavior.

In recent years, the electronic structure of UCu_2Si_2 has been extensively studied by band calculations and x-ray photoemission measurements presenting a model describing the *dual* nature of the $5f$ electrons in this silicide,[9] in line with the earlier considered theory of Zwicknagl *et al.*[10] The electronic structure of all the series of UT_2Si_2 silicides (T stands for a transition metal) first of all can be characterized by the relative energy positions of the d states of a given T atom and the uranium $5f$ states. The tendency to an increase of the difference in these positions weakens the strength of hybridization between these electrons.[11] Thus, in the case of UCu_2Si_2, the d states are the most far away in energy from the Fermi level E_F among all the uranium 1:2:2-type compounds, which causes that the aforementioned hybridization becomes comparably the smallest one just for this silicide.[12–14] Therefore, the U $5f$ states in this silicide are fairly well localized to carry the local magnetic moment and some initial crystal-field treatment of UCu_2Si_2 has been initiated.[15] The crystal field (CF) has been invoked also to explain properties of the other members of the isostructural UT_2Si_2 and UT_2Ge_2

series.[16] Regarding this aspect, among all this family of 1:2:2 systems, there is one silicide, namely, URu_2Si_2, being the most intensively investigated during the last two decades (see a review - Ref. 17). For this compound, various CF ground states and sequences of the lowest excited states, but based on the U^{4+} configuration of the pure $^3H_4$ ground state, have been suggested in order to explain a mysterious hidden order of this phase below $T_0 = 17.5$ K. A large diversity of the models proposed so far[17–19] reflects an unsatisfactory state of the art in a quantitative understanding of the CF effect for this type of compound. This inclines one to investigate both the underlying microscopic mechanisms as well as phenomenological models. The experimental data gathered up to now for UCu_2Si_2 incited us to make a step towards the latter task. It should be mentioned here that except for the CF interaction, a significant Kondo-lattice-like effect due to the interaction of the localized $5f$ electron with the conduction electrons plays here an equally important role.[13–15,20] As far as this ferromagnetic compound is concerned, just the latter behavior is consistent with the recently derived theoretical models of the underscreened Kondo lattice (UKL) or Anderson Kondo lattice (AKL) ones,[21] which describe well the coexistence of both the ferromagnetic and Kondo-type interactions, taken without and with including the hybridization effect, respectively. Thus, based on the band-structure calculations,[9] we also presented there the derived topology of the Fermi surface of UCu_2Si_2, which has allowed us to predict the ILSDW phase mentioned above. Also, the de Haas–van Alphen (dHvA) oscillations measured at 30 mK and in a magnetic field of 17 T on the Sn-flux single crystal of UCu_2Si_2 have revealed several branches which correspond to moderate cyclotron effective masses ranging from 1.4 to $4.2m_0$.[22]

Continuing our previous magnetic and electrical transport bulk studies,[6,13,14] we present in this paper the thermal properties, i.e., the heat capacity and conductivity, performed on a single-crystalline UCu_2Si_2 sample. The former measurements were carried out also in magnetic fields up to 9 T. Furthermore, these measurements were related to the reference compound $ThCu_2Si_2$, which has allowed one to separate the phonon part from the total heat capacity of UCu_2Si_2. The earlier data of the temperature dependencies of the susceptibility and the value of the ordered moment of uranium atom at low temperatures[6] have been reconciled with the results of the calculation model of CF splitting of the uranium ion, using simultaneous diagonalization of all the interactions being active in this tetragonal silicide. The obtained excess in the magnetic heat capacity in the paramagnetic state has been adjusted to both the Schottky-type effect based on the CF level scheme presented in this paper and to the Kondo effect described in our previous paper.[13,14]

II. EXPERIMENT

A single-crystal of UCu_2Si_2 was grown by a self-flux method using Cu as molten flux as described in Ref. 6. The quality of this material was verified by means of x-ray powder diffraction measurements and microprobe analysis using EDAX PV 9800 spectrometer. The measurements of the magnetic susceptibility on a UCu_2Si_2 sample were made in a magnetic field of 0.5 T in the temperature range 1.9–400 K using a small oriented single crystal with dimensions $1.5 \times 1.5 \times 2.5$ mm^3. We used for these measurements a superconducting quantum interference device (SQUID) magnetometer.

The nonmagnetic reference counterpart $ThCu_2Si_2$, as a polycrystalline sample, was obtained by arc melting the stoichiometric components under a titanium gettered argon atmosphere and then by annealing in vacuum at 800 °C for one week (see Refs. 13 and 14). The x-ray powder pattern showed only one phase of tetragonal $ThCr_2Si_2$ type of structure as that of U-based silicide. The lattice parameters of both silicides are given in Refs. 13 and 14.

The heat capacity of the UCu_2Si_2 single crystal and polycrystalline $ThCu_2Si_2$ specimen was measured in the temperature range from 4.2 K up to 300 K by using the thermal relaxation method in the Institute in Wrocław. In addition, the single crystal was measured in applied magnetic fields up to 9 T in the Institute in Karlsruhe. In both cases, Quantum Design PPMS-9 platforms were used. As a sample mounting medium, a vacuum grease Apiezon N was utilized.

The thermal conductivity was measured over the temperature range 5–300 K using the stationary heat-flux method and setting the temperature gradient along the specimen length from 0.1 to 0.5 K. The rectangular specimen was cut from a larger single crystal along the a axis with typical dimensioms of about $1 \times 1 \times 2.5$ mm^3. The uncertainty in measurements was not higher than 3%.

III. RESULTS AND DISCUSSION

A. Localized nature of $5f$ electrons in tetragonal 1:2:2 uranium compounds

In the body-centered-tetragonal $ThCr_2Si_2$ structure (space group $I4/mmm$), the U atoms are located at $z = 0$ and $\frac{1}{2}$, Cu at $\frac{1}{4}$ and $\frac{3}{4}$, and Si at ± 0.3823, i.e., close to $\frac{3}{8}$.[13,14] This structure can be presented as a sequence of layers having the same kind of atoms stacked in the direction of the tetragonal axis. The coordination around the uranium (or thorium) central atom of Cu and Si atoms with the D_{4h} point symmetry is presented in Fig. 1. As seen, the coordination number (CN) is 16 (8Si + 8Cu). The uranium atom is surrounded by silicon

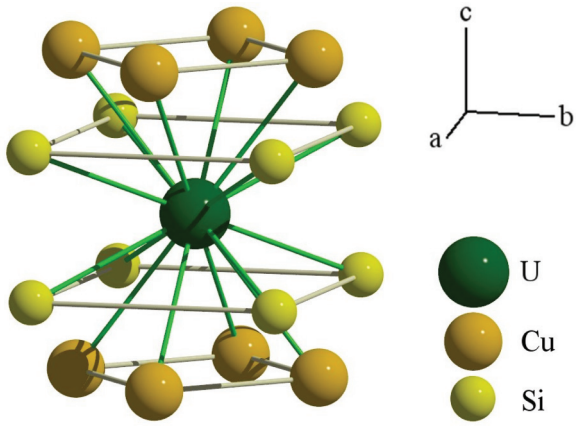

FIG. 1. (Color online) Coordination polyhedron of uranium atom in UCu_2Si_2.

atoms (at interatomic distances of 0.3052 nm) which are located on the corners of the flattened cube [USi_8]. At the same time, the $CuSi_4$ tetrahedra, where Cu–Si distances are equal to 0.2388 nm, are strongly covalently bounded, as indicated by crystal orbital overlap population (COOP) calculations implemented within the augmented spherical wave (ASW) method.[23] The U–Cu bonds of 0.3186 nm may also play some role if one takes into account the associated charge distribution being quite different from that of the U–Si bonds. All these structural considerations made for UCu_2Si_2 point to a large degree of localization of the $5f$ electrons in this silicide with only their weak hybridization with the $3d$ electrons, while usually neglecting the p-f mixing mechanism.[24] As pointed out by Żołnierek and Mulak,[16] the latter may markedly influence the $5f$-electron magnetism in all the series of $UT_2(Si,Ge)_2$ ternaries. In general, one can expect a competition between the single-ion CF and two-ion exchange anisotropy.[25] On this basis, the above authors[16] have predicted the key role of the CF effects in understanding the magnetism of all uranium 1:2:2 tetragonal ternaries.

In order to accomplish any CF calculations, the uranium valence state in UCu_2Si_2 or related tetragonal compounds are needed. So far in the family of 1:2:2 ternaries, the most intense CF calculations, but assuming the Russel-Saunders coupling, have been undertaken for URu_2Si_2 (see a review paper of Ref. 17). Concerning the temperature dependence of the susceptibility, a localized picture involving the CF scheme assuming the $5f^2$ configuration was proposed for this silicide.[26,27] Taking into account the lowest-lying three singlets, e.g., Γ_{t3}, Γ^1_{t1}, and Γ_{t4}, the authors could reproduce a maximum in the susceptibility for the [001] direction and explain the strong uniaxial magnetic anisotropy in the susceptibility data. A strong Ising-type anisotropy was also observed in the study of diluted uranium solid solutions $U_xTh_{1-x}Cu_2Si_2$, where the CF state doublet Γ_{5t} was taken as a ground state.[28] Moreover, the authors suggested that the observed non-Fermi-liquid behavior of their diluted compositions could be described by the two-channel Kondo effects in the tetragonal symmetry. In turn, Galatanu *et al.*[29] considered in the case of URu_2Si_2 the two CF schemes, i.e., the $5f^2$ and $5f^3$ configurations, assuming in both cases a doublet ground state. The total CF splittings of the ground multiplet $^3H_4$ for these cases were 3613 and 1761 K, respectively, which led, however, to very similar temperature behavior of the theoretical reciprocal susceptibilities, compared to those measured on a single crystal up to 800 K in the [001] and [100] directions.

In our CF consideration of the uranium-ionic state in UCu_2Si_2, we first analyze Fig. 1 of Ref. 30, where the unit-cell volumes of the tetragonal RCu_2Si_2 series of compounds, where R is a rare-earth element or Th, have been plotted as a function of the respective ionic radii, taken from Ref. 31 for R^{3+} and Th^{4+} ions. All stable 1:2:2 compounds in this plot form a well-defined line. Taking our unit-cell volumes (V's) equal to 0.158 nm^3 for UCu_2Si_2 and 0.166 nm^3 for $ThCu_2Si_2$, one can easily find from this plot a uranium and thorium ionic radius of 0.092 and 0.102 nm, in these silicides, respectively. These values are, in turn, close to those given by Shannon[32] for U^{4+} (0.089 nm) and for Th^{4+} (0.094 nm) ions. Hence, the $5f^2$-electron configuration characteristic of the U^{4+} ion should be the most probable one for UCu_2Si_2. Nevertheless, we have probed also the $5f^3$-electron configuration. It has not led, however, to results of a comparable quality with those obtained for $5f^2$.

B. Crystal-field model

Following the above remarks on admixture of the dispersive states, for the energy scale restricted to room temperature, the perturbation theory can be probed with the effective renormalized Hamiltonian operating in the space of purely localized wave functions with the conventional one-electron effective CF potential. For the actual D_{4h} ($4/mmm$) point symmetry (Fig. 1), this potential can be represented by five parameters B_{20}, B_{40}, B_{44}, B_{60}, and B_{64} appearing in the Wybourne expansion in terms of the normalized spherical harmonics $\hat{C}^{(k)}_q$ (Ref. 33):

$$\hat{h}_{\mathrm{CF}}(\mathbf{r}/r) = \sum_{k,q} B_{kq}\hat{C}^{(k)}_q(\mathbf{r}/r). \tag{1}$$

The B_{kq} parameters in Eq. (1) should not be mixed up with those used in the more common equivalent Stevens operators method[34] according to which the CF Hamiltonian acts on the two-electron functions restricted to the ground $^3H_4$ multiplet in the pure Russel-Saunders coupling scheme.

To reproduce more reliably the internal structure of the $5f^2$ states of the uranium atom, the onsite correlations due to the Coulomb interaction and the relativistic correction at least of the lowest order have to be taken into account. It has been evidenced that in the case of uranium compounds, even moderate admixture (10%–20%) of the higher multiplets to the ground $^3H_4$ multiplet may result in a drastic modification of the CF level scheme[35] including the ground state and the arrangement of the lowest excited levels. Such a modification may be crucial for the observed magnetic, transport, and thermal properties. Thus, in the wave-function subspace projected to the pure $5f^2$ states, the effective parametric Hamiltonian apart from the CF potential must include both the "free-ion" interactions, namely, Coulomb and spin-orbit ones, renormalized on account of the projection to the ground $5f^2$ configuration:

$$H_{5f} = \sum_k F^k \hat{f}_k + \zeta_{5f}\sum_i \mathbf{l}_i\cdot\mathbf{s}_i + \sum_i \hat{h}_{\mathrm{CF}}(\mathbf{r}_i/r_i) + \sum_i \mu_{\mathrm{B}}(\mathbf{l}_i + 2\mathbf{s}_i)\cdot\mathbf{B}, \tag{2}$$

where the "free-ion" parameters F^k, $k = 2, 4, 6$, and ζ_{5f} describe the Coulomb repulsion and the spin-orbit coupling constants, respectively. The fourth term in (2) turns on the external ($\mathbf{B}_{\mathrm{ext}}$) and/or internal [molecular, ($\mathbf{B}_{\mathrm{int}}$)] magnetic field $\mathbf{B} = \mathbf{B}_{\mathrm{ext}} + \mathbf{B}_{\mathrm{int}}$, $\mathbf{B}_{\mathrm{int}} = \lambda\mathbf{M}$, where $\mathbf{M}$ is the spontaneous magnetization and λ is the molecular field constant. The operators $\hat{f}_k$ are the angular parts of the Coulomb interaction, $\mathbf{l}$ and $\mathbf{s}$ are the orbital and spin angular momentum operators of the f electron labeled i, and μ_{B} is the Bohr magneton. For the free-ion parameters, we took values from Ref. 36 and do not vary them during the fittings. All the four main interactions in Eq. (2) are diagonalized simultaneously in each cycle of the fitting procedure in which the B_{kq} parameters and the molecular field constant λ are varied so

as to reproduce the experimental temperature dependencies of three quantities, i.e., the perpendicular ($\chi_\perp$) and parallel ($\chi_\parallel$) magnetic susceptibilities:

$$\chi_{\mathrm{mol},\alpha} = \frac{N_\mathrm{A}}{B_\alpha} \frac{\sum_\nu \mu_{\nu,\alpha} \exp\left(-\beta E_{\nu,\alpha}\right)}{\sum_\nu \exp\left(-\beta E_{\nu,\alpha}\right)}, \tag{3}$$

where

$$\mu_{\nu,\alpha} = -\frac{\partial E_{\nu,\alpha}}{\partial B_\alpha} \tag{4}$$

and $E_{\nu,\alpha}$ are the eigenvalues of the Hamiltonian (2). The index α denotes direction of the magnetic field (parallel $\parallel$ or perpendicular $\perp$ to the easy axis) and the Schottky contribution to the specific heat given by Eq. (7) in the next section.

In the ordered phase, the molecular field has been determined self-consistently for each temperature point. For the whole temperature range, the experimental points have been entered with appropriate weights with regard to accuracy of the measurements.

From the mathematical point of view, for each of N temperature points, we have three experimental quantities. These quantities depend on the sequence of quantum states being efficient in the considered energy scale with weights determined by the temperature. The states in turn are determined by the CF Hamiltonian. Thus, mathematically we have $3N$ nonlinear equations from which we determine the 5 CF parameters and the molecular field constant. Of course, these equations are not independent. Moreover, they may generate unphysical solutions corresponding to local minima of the root-mean-square error being minimized during the fittings. That is why we started with the simplified, two-parameter approach. Then, the extended, four-parameter model was applied and finally the results were refined with the ordinary five-parameter model.

The initial set of parameters has been generated using the angular overlap model (AOM) in the way described previously for UGe_2.[37] In this simplified model, the role of the CF parameters is played by energies of metal-ligand interaction of various symmetries e_σ, e_π, and e_δ corresponding to the absolute value of the $5f$ magnetic quantum number $\mu_i = |\mu|$ equal to 0, 1, and 2, respectively. The e_μ parameters relate to the ordinary B_{kq} parameters through the formula

$$B_{kq} = \sum_\mu W_{kq}^{\mu(\mathrm{Si})} e_\mu^{\mathrm{Si}} + \sum_\mu W_{kq}^{\mu(\mathrm{Cu})} e_\mu^{\mathrm{Cu}}, \tag{5}$$

where the coordination factors $W_{kq}^{\mu(\mathrm{Si})}$ and $W_{kq}^{\mu(\mathrm{Cu})}$ absorb the whole information about the geometry of the $[USi_8]$ and $[UCu_8]$ coordination polyhedra, respectively (for further details, see Ref. 38). We calculated these factors using the crystallographic data from Refs. 13 and 14. Since, unlike for the binary UGe_2, two completely different atoms Si and Cu appear in the neighborhood of the uranium atom (see Fig. 1) in UCu_2Si_2, a minimum of two independent parameters among six ones, describing the interactions with each of them, are required, i.e., one parameter at least should represent each of the ligands. In preliminary calculations, various combinations of the e_μ parameters have been probed in the fitting. The most promising sets of AOM parameters obtained in this step have been converted according to Eq. (5) to the corresponding sets of the B_{kq} parameters. The latter in turn have been treated as starting ones in the final step of the calculations. All the fittings have been performed using the program CONDON (Ref. 39) extended so as to include the three parameters per nonequivalent ligand of the AOM approach and the Schottky contribution to the specific heat.[40] A final set of model parameters has been selected from a few solutions of similar quality so as to minimize both the average and maximum errors with respect to the experimental temperature dependencies.

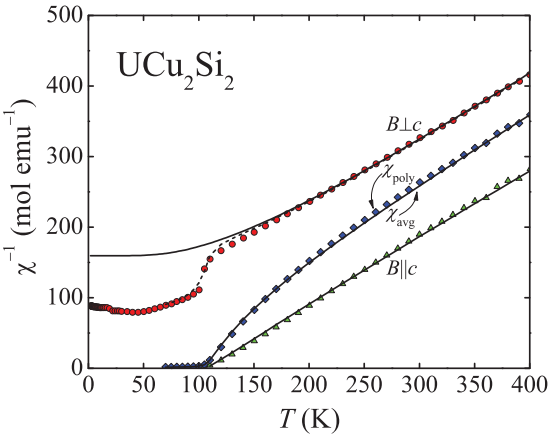

FIG. 2. (Color online) Experimental (points) and model (lines) reciprocal magnetic susceptibilities for UCu_2Si_2 against temperature. The susceptibility χ_{avg} averaged over two field directions is compared to that of χ_{poly} measured on the polycrystalline sample. The dotted line is the calculated curve after rotation of the hard direction only by 0.15° out from the perfect orientation to account for the experimental points in the vicinity and below T_C.

As seen in Fig. 2, our model reproduces the reciprocal magnetic susceptibility satisfactorily for both the easy c and hard a directions. Characteristic divergence from the calculated curve seen for the hard a direction around T_C and below results from an imperfect orientation along the hard direction of the single-crystalline sample during the measurements. It was enough to rotate the coordinate system by only 0.15° to restore precisely the observed deviation in the reciprocal perpendicular susceptibility from the expected temperature dependence (solid line), as shown by dotted line in Fig. 2.

The molecular field constant λ was established to be equal to 82.7 mol emu^{-1}. The Schottky contribution to the heat capacity combined with the remaining contribution of Kondo-like type, discussed in details in the next section, also agrees well with the experimental data. The energies and compositions of the eigenfunctions of the states relevant for the experimental data used in the fitting are shown in Table I. As many as five levels, two doublets and three singlets, are grouped below 800 K determining the thermodynamic properties in the whole temperature range under consideration. As seen in Table I, the doublet Γ_5 is the ground state that carries the ordered moment of $1.85\mu_\mathrm{B}$. Thus, the calculated value was found to lie in the range of experimental values reported elsewhere (1.6–$2.0\mu_\mathrm{B}$, see Refs. 13 and 14 and references therein). The model value of the ordered magnetic moment at 0 K can be regarded as an additional test of the reliability of the fitting of the thermodynamic quantities at the lowest and elevated temperatures. The two lowest excited levels are singlets placed

TABLE I. The model electronic states in the $^{2S+1}L_J$ basis and the eigenvalues (in K) of the localized electron subsystem obtained using the effective Hamiltonian (2) and the refined CF parameters shown together with the initial ones obtained within the AOM approximation.

	B_{kq} (in K)	
kq	AOM[ab]	Refined[c]
20	−233	857
40	−17 995	−9180
44	−12 678	−7405
60	19 164	14 550
64	−22 677	−17 233

Irrep. state	Energy (K)	$^3H_4$ components of the eigenstates[d]
Γ_5	0	$\pm 0.9132\|^3H_{4\pm3}\rangle \mp 0.3073\|^3H_{4\mp1}\rangle$
Γ_1	295	$0.7264\|^3H_{40}\rangle + 0.4113\|^3H_{44}\rangle + 0.4113\|^3H_{4-4}\rangle$
Γ_4	327	$-0.6756\|^3H_{42}\rangle + 0.6756\|^3H_{4-2}\rangle$
Γ_2	700	$0.6288\|^3H_{44}\rangle - 0.6288\|^3H_{4-4}\rangle$
Γ_5	774	$\pm 0.8355\|^3H_{4\pm1}\rangle \pm 0.2652\|^3H_{4\mp3}\rangle$
Γ_1	2028	$-0.5656\|^3H_{40}\rangle + 0.5062\|^3H_{4-4}\rangle + 0.5062\|^3H_{44}\rangle$
Γ_3	2762	$-0.6125\|^3H_{42}\rangle - 0.6125\|^3H_{4-2}\rangle$

[a]The molecular field constant λ obtained from the AOM and the refined calculations is the same and equal to 82.7 mol/emu.

[b]The following AOM parameters have been obtained: $e_\pi^{Cu} = 4663$ K, $e_\delta^{Cu} = -1427$ K, $e_\sigma^{Si} = 2487$ K, $e_\pi^{Si} = 5344$ K. These values have been converted according to Eq. (5) to the B_{kq} parameters shown in column AOM.

[c]The values of the Slater integrals and the spin-orbit coupling parameters were fixed at the following values (Ref. 36): $F^2 = 61\,376$ K, $F^4 = 56\,803$ K, $F^6 = 35\,176$ K, $\zeta = 2482$ K.

[d]Only the components of the main $^3H_4$ term of the ground mutiplet are shown. The remaining $^{2S+1}L_J$ mutiplets altogether contribute up to over 30% for some CF levels.

at about 300 K and the next two levels, i.e., the singlet and doublet, are placed in the region of 700–800 K. Further, two levels are located above 2000 K so they are responsible for the anisotropy still apparent at 400 K and for a divergence of the effective moment characterizing the slope of the reciprocal susceptibility curve leading to the effective magnetic moment of about $3.0\mu_B$ along both considered directions here.[6] The latter value may be compared to the free-ion value of $3.63\mu_B$ in the case of the intermediate coupling scheme.

The final CF parameters are given in Table I. As for URu_2Si_2 (Ref. 29) and UGe_2 (Ref. 37), the CF parameters are relatively large (in their absolute values). The large CF effect in presence of screening conduction electrons may raise some doubts if one thinks in terms of electrostatic forces. Actually, the pure quantum effect (the hybridization) provides the leading contribution. Its magnitude depends on the difference between the Fermi energy and the ground-state energy of the localized electrons. If these energies are sufficiently close to each other as for the whole UT_2Si_2 family of compounds, the hybridization contribution grows up yielding a large CF effect (see Ref. 41). The corresponding total CF splitting of the ground multiplet amounts to 2761 K, the value being close to that obtained previously for UGe_2 (2864 K) (Ref. 37) and smaller than 3613 K reported for URu_2Si_2 from analogous analysis.[29] We have checked that the fourth-rank CF components alone, similarly to the sixth-rank components, both produce separately the splittings of the ground multiplet being larger than that of the total splitting. This is because the fourth- and sixth-rank contributions taken together cancel to some extent each other. In turn, the second-rank term is relatively small, which is not unusual in the case of the uranium systems. The initial B_{kq} parameters (shown in Table I), which have been obtained from the preliminary AOM fittings, have occurred to be close to those of the final ones. Looking at the values of the AOM parameters alone (see footnotes in Table I), we see that the regularity of the AOM parameters characteristic of an ionic system[41] is not observed for UCu_2Si_2. They are also quite different from those reported previously for UGe_2. Probably the competing mechanisms responsible for the CF effect in the case of the two electron subsystems, localized and itinerant ones[41] in which the localized states lie in the vicinity of the Fermi energy of the conduction band, fluctuate sharply with even slight differences appearing in chemical potentials of these subsystems. Two of them, just the most important CF mechanisms, namely, the hybridization and formation of a virtual bond state, are especially sensitive from their very nature to the energy separation of the localized and virtual states with respect to the Fermi energy. Thus, for the U–Cu linear ligator, we get a large, positive $e_\pi^{Cu} = 4663$ K and negative $e_\delta^{Cu} = 1427$ K. In the case of the U–Si interaction, e_σ^{Si} reaches a value of 2487 K, being typical of an ionic linear ligator, but e_π^{Si} grows up to 5344 K. Thus, a question arises as to how reliable these calculations are. To answer this question, we first present shortly our calculation procedure applied. We start with all the possible combinations of only two parameters: the first one for U–Cu among e_μ^{Cu} ($\mu = \sigma, \pi, \delta$) and the second one for U–Si among e_μ^{Si} ($\mu = \sigma, \pi, \delta$). The best solution has been obtained with nonzero e_π^{Cu} and e_π^{Si}. Starting with these two values we have then probed all the eight combinations of the remaining parameters (=3 × 3 − 1, i.e., excluding the case of six AOM parameters as exceeding the maximum number of independent parameters admitted by the D_{4h} point symmetry). The final four AOM parameters given above have provided a quite satisfactory solution. It has turned out that further release of e_σ^{Cu} or e_δ^{Si} led only to a negligible correction which did not improve the fitting noticeably, so we kept them zero. As mentioned above, these four AOM parameters have been converted to the usual B_{kq} parameters and served as an initial set in the refining fitting.

C. Heat capacity

Previous heat-capacity measurements of UCu_2Si_2 were a subject of interest of several authors. Fisk *et al.*[8] carried out such measurements on their single crystal, obtained by the Cu-flux method, which had a form of a millimeter-size plate. They found on the $C_p(T)$ dependence two not very large transition peaks, one at T_C (≈96 K) and the second at T_N (≈100 K). In turn, Matsuda *et al.*[7] using their flat single crystal of a small size (1.6 × 1.5 × 0.7 mm^3), obtained by the Sn-flux method, have reported also two transitions in $C_p(T)$, but at corresponding temperatures being a little higher, i.e., at 100 and 106 K, respectively. Although both the peaks are

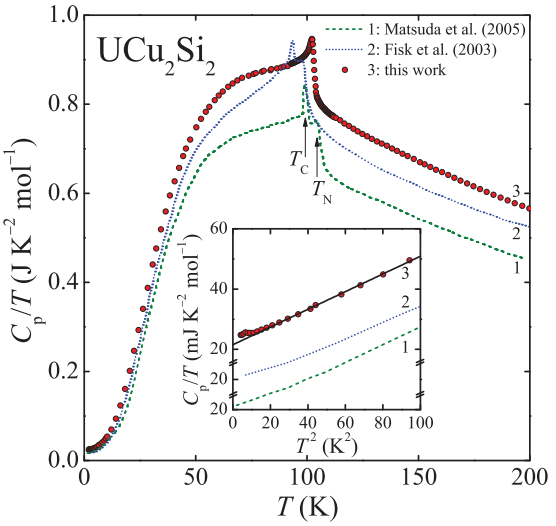

FIG. 3. (Color online) Temperature dependencies of the heat capacity of UCu_2Si_2 in C_p/T vs T presentation measured by the three groups of authors indicated in the figure. The inset gives the low-temperature presentation of C_p/T vs T^2 data reported by these groups.

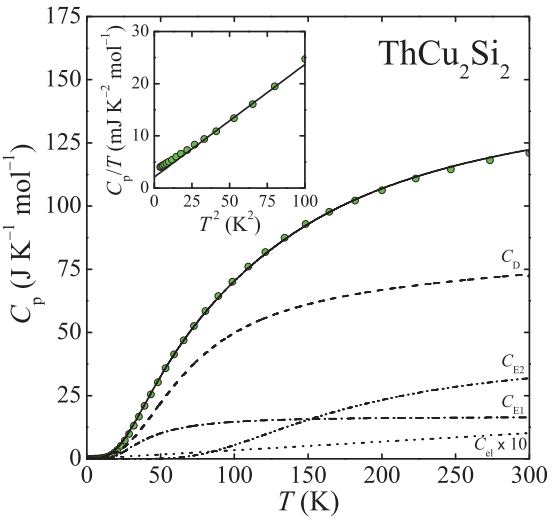

FIG. 4. (Color online) Temperature dependence of the heat capacity C_p vs T of $ThCu_2Si_2$. The phonon part of this dependence $C_{ph}(T)$ was analyzed using the sum of the Debye and Einstein approaches [see Eq. (6)]. The full line displays the sum of the best fits of the phonon and electronic contributions, i.e., $C_{ph} + C_{el}$, to the measured heat capacity C_p of this silicide. The inset shows the low-temperature C_p/T vs T^2 plot.

also small, the authors claimed that the former transition is of the first-order one. We have decided to reexamine also our single crystal by a heat-capacity treatment. As we have already mentioned in the Introduction, our previous magnetic[6] and transport[13,14] measurements indicated only one magnetic transition just at T_C (=103 K). Such an unexpected result we have accounted by the simultaneous coexistence of the ferromagnetic phase of a localized character with the coupled spin-density wave (SDW) and charge-density wave (CDW) phases of an itinerant character. This phase, however, due to a strong molecular field created by the local-ferromagnetic-type phase, can only be revealed by showing a huge negative magnetoresistance and some excess in $C_p(T)$ below T_C. Therefore, the latter observation, which corresponds to a case that $T_C \approx T_N$, is probably brought about by the existence below T_C of strong SDW/CDW-type fluctuations (for details see Refs. 13 and 14).

In Fig. 3, we have compared all the three $C_p(T)/T$ curves described above, drawn only up to 200 K. As seen, there exists, in the lower-temperature range, a reasonable accord in the C_p/T data of all the three measurements with one another. However, all these three curves at higher temperatures become quite divergent from one another, probably due to some differences in compositions. As we will show in the following, only our heat-capacity measurements of UCu_2Si_2 were done up to room temperature (RT). Thus, our heat-capacity results at RT have confirmed to be only slightly above that expected from the Dulong-Petit (DP) rule (see below). The C_p/T versus T^2 plots (see the inset to this figure) give rise to almost the same values of 21(2) $mJmol^{-1}$ K^{-2} for the linear electronic heat-capacity term $\gamma^U(0)$ for these three cases, but taken for all of them above 5 K. Some low-temperature (LT) deviation from the linear behavior observed below this temperature is probably caused by impurities. The determined by us low-temperature Debye temperature $\Theta_D^U \approx 330(10)$ K is a little lower than that established in Ref. 8 (348 K) by an extrapolation from the lower applied temperature range (1–4) K and, hence, being higher than our Θ_D^U.

To consider the magnetic contributions into the total C_p of UCu_2Si_2, first we concentrate ourselves on the isostructural silicide $ThCu_2Si_2$. The $C_p^{Th}(T)$ curve for this nonmagnetic compound, taken up to 300 K, is presented in Fig. 4. The $\gamma^{Th}(0)$ value and LT Debye temperature Θ_D^{Th} are 2.6(5) $mJmol^{-1}$ K^{-2} and 350(10) K, respectively (see the inset to Fig. 4). In this case, we have to do only with the phonon and electronic contributions. After separation of a small part of the latter, the resulted heat capacity will be used by us as the phonon contribution $C_{ph}(T)$ of UCu_2Si_2, neglecting the fact of a very small difference (1.5%) in their molecular masses.

As shown in this figure, the RT heat capacity of $ThCu_2Si_2$, containing atoms 5 atoms/f.u., reaches almost a value expected from the DP law of $5 \times 3R = 15R$, i.e., 124.7 $Jmol^{-1}$ K^{-2} (where R is the gas constant). We were able to describe the phonon heat capacity of this Th-based compound only by splitting its phonon spectrum into the acoustic and optical branches as, e.g., it was done in the cases of $ThNi_2Si_2$ (Ref. 42) or $ThGe_2$ (Ref. 37). Thus, the next step is to get the first Einstein temperature Θ_{E1}. For this purpose, we have considered the function C_p/T^3 versus T (not shown here), as it was done in the case of $ThGe_2$ (see the inset to Fig. 7 in Ref. 37). From the temperature of the maximum in this function, observed at $T_{max} = 25$ K, we get $\Theta_{E1} \approx 125$ K, characterizing C_{E1}. Thus, the smooth curve (thick line), obtained by fitting Eq. (6) to the experimental data, is composed approximately of four fitting terms:

$$C_p^{Th} = C_D + C_{E1} + C_{E2} + C_{el}. \quad (6)$$

In this formula, the acoustic phonons C_D are described by the three Debye modes [but here with the average Debye temperature Θ_D (=276 K)]. In turn, the optical phonons ($C_{E1,2}$)

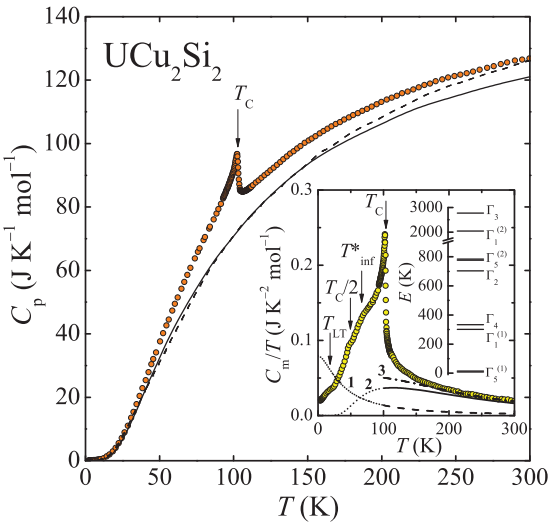

FIG. 5. (Color online) Temperature dependencies of measured heat capacity of UCu_2Si_2 (circles) and phonon parts of $ThCu_2Si_2$ (solid line) and $ThNi_2Si_2$ (dashed line). The latter is taken from Ref. 42. The inset presents the extracted magnetic and electronic parts in the form of the C_m/T vs T dependence. The temperatures of four detected anomalies described in the text are marked. Above T_C (=103 K) both the Kondo-like (dashed line, No. 1) and Schottky-type (solid line, No. 2) contributions (see the text) are shown. The dotted-dashed line (No. 3) is a sum of both contributions. The dotted lines indicate the temperature variations of the above two types of contributions in the case of the lack of the magnetic order. In addition, this inset also gives the calculated CF energy level scheme.

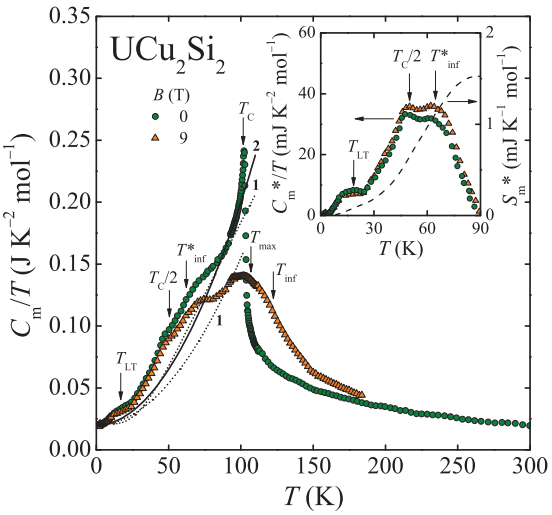

FIG. 6. (Color online) Temperature dependencies of the magnetic heat capacities of UCu_2Si_2, in the form of $C_m(T)/T$ (including the electronic part) extracted from the heat-capacity data taken at zero field and 9 T by subtracting the phonon part. Curves No. 1 (solid line) and No. 2 (dotted line) represent the magnon behavior according to Eqs. (9) and (10), respectively. The inset gives the extracted magnetic parts (humps) obtained at zero field and 9 T, attributed to the itinerant subsystems of $5f$ electrons. The dashed line presents the temperature magnetic entropy variation of the itinerant hump.

are characterized by 12 Einstein modes, but here we represent them by the two average Einstein temperatures: Θ_{E1} (derived from T_{max}) and $\Theta_{E2} = 540$ K. The weights for these three components are $\frac{8}{3}$, $\frac{2}{3}$, and $\frac{5}{3}$, respectively. Respective formulas to calculate the Debye and Einstein contributions were given in Ref. 37. As seen from Fig. 4, the fit taken together with very small C_{el} gives a satisfying result.

In Fig. 5, we present both the measured heat capacity of UCu_2Si_2 in the form of $C_p^U(T)$ (points) and $C_{ph}(T)$ (solid line), taken as the difference $C_p^{Th}(T) - C_{el}^{Th}(T)$. In turn, the difference between the two curves shown in this figure yields the magnetic part $C_m(T)$. The latter divided by T is displayed in the inset to this figure. For comparison, in Fig. 5 we have also plotted (dashed line) the curve representing the phonon part derived in Ref. 42 for the isostructural silicide UNi_2Si_2. As seen, this curve starts to exceed our corresponding curve at about 150 K and at RT the DP limit is significantly surpassed. To get a value close to that expected from this limit, the authors of that work have introduced the anharmonic terms into their analysis of the thermal data. It is interesting to underline that we have not needed to use this type of the correction. However, our not-corrected $C_{ph}(T)$ curve follows very well their one but after introducing by them the correction mentioned above (not shown here).

The inset to Fig. 5 presents the extracted magnetic and electronic parts in the form of one C_m/T versus T dependence obtained by subtracting the phonon data (based on the reference compound $ThCu_2Si_2$) from the measured heat-capacity data of UCu_2Si_2. As is seen in this inset, the above temperature dependence with increasing temperature goes by several anomalies described successively by T_{LT}, $T_C/2$, T^*_{inf}, and, finally, by only one sharp peak (compare it with Fig. 3 and the inset to Fig. 6) at T_C of 103 K. Some description of these revealed anomalies will be given in the following. Above T_C, this dependence is fitted to both the Schottky-type (solid line) and Kondo-like (dashed line) contributions. The former has been calculated by means of

$$C_{Sch}(T) = \frac{dF}{dT} = \frac{R}{T^2}\frac{\sum_i e^{-E_i/T}\sum_i E_i^2 e^{-E_i/T} - \left[\sum_i E_i e^{-E_i/T}\right]^2}{\left[\sum_i e^{-E_i/T}\right]^2} \quad (7)$$

and using the CF level scheme discussed above. Apart from the CF effect reflected in the $C_m(T)/T$ curve, we also have to do here with the Kondo-like interactions which were indicated by the electrical resistivity measurements reported in our previous paper concerning UCu_2Si_2.[13,14] Interestingly, its homologue UCu_2Ge_2 is also a ferromagnet ($T_C = 107$ K) and exhibits the Kondo-lattice properties documented among others by the dependence of its critical temperature on pressure.[43] The latter is reminiscent of the well-known Doniach magnetic phase diagram. These interactions also introduce its heat-capacity account, visualized in the paramagnetic region, by producing a C_K excess into the total magnetic heat capacity C_m (see, e.g., Ref. 44). According to Schotte and Schotte,[45] the Kondo-type contribution C_K with an effective spin $S = \frac{1}{2}$ can be described by the formula

$$C_K\left(\frac{T}{T_K}\right) = 2R\frac{T_K}{2\pi T}\left[1 - \frac{T_K}{2\pi T}\psi'\left(\frac{1}{2} - \frac{T_K}{2\pi T}\right)\right], \quad (8)$$

where R is the universal gas constant, ψ' is the derivative of the digamma function, and T_K is the Kondo temperature of the system, defined as the width of the Lorentzian-shaped Kondo resonance at the Fermi level. This contribution, divided by T, shown in the inset of Fig. 5, has been calculated for $T_K = 110$ K, taking into account the difference in the heat capacities between C_m and C_{Sch} in the paramagnetic region of temperatures and neglecting in this region the electronic part C_{el}^U which should be here quite negligible. Thus, the dotted-dashed line is the sum of both contributions, i.e., $C_{Sch} + C_K$. Shown also in this inset, the dotted lines indicate the temperature variations of the above two types of the contributions in the case of the lack of any magnetic order. Interestingly, the extrapolation of the $C_K(T)/T$ function to $T = 0$ K yields a value of about 80 mJmol^{-1}K^{-2}. A similar value was obtained in the case of UGe_2.[37] It is likely that the ferromagnetic order revealed in these two materials, i.e., in UCu_2Si_2 and UGe_2, depresses down that value to those measured ones, namely, $\gamma^U(0) = 21$ and 33 mJmol^{-1}K^{-2}, respectively. This fact is also consistent with the presence of Kondo-type interactions in the ferromagnetic materials, as predicted by the theory.[21]

It is worth noting that the Schotte-Schotte model[45] is originally a phenomenological approach to the density of states at the Fermi level and a $\frac{1}{2}$-effective spin. Although this model is not the exact theory of the Kondo problem, it yields in the analytical form nearly the same results as the troublesome numerical solution of the $s-d$ model of the onsite Kondo interaction.[46] So, Eq. (8) allows us to determine fairly easy the Kondo contribution $C_K(T)$ to the total magnetic part of the heat capacity in UCu_2Si_2.

As seen from Fig. 5, the $C_m(T)/T$ curve increases markedly when approaching T_C from higher temperatures due to effects of the Kondo- and magnetic-critical types of fluctuations and/or installing a short-range magnetic order. For the purpose of discussing the magnetic part of the heat capacity of UCu_2Si_2 in the ferromagnetic temperature region in greater detail, we again display in Fig. 6 the C_m/T versus T dependence separated above. Additionally, we have plotted in this enlarged figure such a dependence (isolated by means of the procedure described above) but taken in an applied field of 9 T and at temperatures up to 180 K. As seen, the anomalies mentioned above as an effect of the itinerant part of the $5f$ electrons of uranium atoms in UCu_2Si_2 (see our previous papers in Refs. 13 and 14) are here more distinctly presented. It is clear from this figure that the complex shape of the C_m/T versus T dependence is brought about owing to the dual character of the $5f$ electrons of uranium atoms. Furthermore, we will try to extract this additional hump from $C_m(T)/T$ data, attributed to the itinerant subsystem $C_{m,itin}/T$ by forming the typical magnon functions reflected in the localized $5f$-electron subsystem $C_{m,loc}/T$. We can do it only approximately because in the fitting we deal only with a few experimental data at the low- and high-temperature ranges. To find the temperature dependence of the latter, we have attempted to use the two different formulas (9) and (10), describing the magnetic heat capacity in UCu_2Si_2 implied by ferromagnetic magnons with including an energy gap Δ in their dispersion relations, as given in the following:

$$C_{m,loc}(T)/T = \gamma^U(0) + aT^2 \exp -\frac{\Delta}{T} \quad (9)$$

or

$$C_{m,loc}(T)/T = \gamma^U(0) + bT^{1/2} \exp -\frac{\Delta}{T}. \quad (10)$$

The fits made to these two equations have been done up to 90 K. One gets the satisfying fit by using the first equation with $a = 1.8 \times 10^{-5}$ and 1.3×10^{-5} J mol^{-1} K^{-4} for the zero-field and 9-T curves, respectively, while $\gamma^U(0)$ (=21 mJmol^{-1}K^2) and Δ ($\approx$0 K) for both cases were taken with the same values (curves No. 1). The second equation we used only for the zero-field case getting $b = 0.04$ Jmol^{-1}K$^{3/2}$ and $\Delta \approx 90$ K (curve No. 2) with the electronic coefficient $\gamma^U(0)$, taken as above. In the inset to this figure, we have plotted an extracted hump obtained from the difference: $C_{m,itin}(T)/T = C_m(T)/T - C_{m,loc}(T)/T$. As seen further from Fig. 6, the zero-field curves Nos. 1 and 2 differ negligibly from each other up to 5 K and, therefore, do not practically change the temperature dependence of the magnetic entropy $S_m^*(T)$ attributed to the heat-capacity hump, as shown also in this inset by one dashed curve. At 90 K, S_m^* (at 0 T) can be roughly estimated as about 1.5 mJmol^{-1}K^{-2}. This value can be compared to that of 0.28 mJmol^{-1}K^{-2}, found previously for such a hump in the magnetic heat capacity of UGe_2.[37] Interestingly, the corresponding hump observed in the latter case goes only by one simple maximum at $T_C/2$. Now, we discuss all the anomalies appeared in the extracted zero-field and 9-T humps of UCu_2Si_2 both being visualized in the above inset. Surprisingly, there are as many as three maxima formed at T_{LT}, $T_C/2$, and T_{inf}^*. The lower-temperature anomaly seems to be not changed by applying a magnetic field of 9 T [no change of the $\gamma(0)$ value at 9 T], while the two others not only do not show at this field any variation with their T_{max}, but only exhibit a slight change in their sizes, implying merely a small difference in $S_m^*(T)$ (at 9 T) compared to that in the zero-field one (not shown). Based on the electrical transport and thermal properties described for UGe_2,[37] we expected in UCu_2Si_2 a similar behavior of displaying the one maximum at T^* ($\approx T_C/2 = 51.5$ K). Now, it is clear that in contrast to UGe_2, the itinerant subsystem in the silicide displays in its thermal properties except for that at T_{LT} the two maxima: at $T_C/2$ and T_{inf}^* ($\approx$65 K). It is interesting to add that, due to the diffused anomalies observed in the transport properties of the UCu_2Si_2 single crystal,[13,14] it was difficult to recognize these two maxima earlier and we determined only T_{inf}. At present, we do not have any explanation for these multiple occurrences of these anomalies.

In Fig. 7, we have plotted the temperature dependencies of the total magnetic entropy $S_m(T)$ (containing the electronic part), calculated by integrating $C_m(T)/T$ up to 300 K (solid line) and 180 K (dashed line) found in the zero-field and 9-T experiments, respectively. As can be seen in this figure, this function at zero field goes at T_C by a distinct kink and the entropy at this transition point amounts between $R \ln 3$ and $R \ln 4$, i.e., about 10 mJmol^{-1}K^{-1}. This value is much higher than that reported for UNi_2Si_2 ($R \ln 2$) at T_N (=124 K).[42] In general, one can not make such a direct comparison due to a large variety of procedures which are

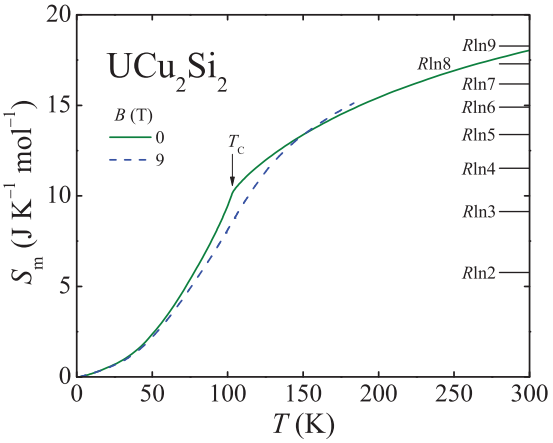

FIG. 7. (Color online) Temperature variation of the total magnetic entropy $S_m(T)$ taken at zero field (solid line) and 9 T (dashed line).

applied by different authors in discussing their heat-capacity data. Our result, though, significantly overpasses the $R\ln 2$ value corresponding to our ground-state doublet, but it likely covers also the influence of higher-lying CF levels, split by the molecular field below T_C. Moreover, it also includes the presence of short magnetic order and some increase in the Kondo effect just close to T_C beside the electronic heat-capacity component, which was not subtracted. The latter always brings an important problem because actually we do not know how C_{el} depends on temperature. As is also seen from Fig. 7, $S_m(T)$ instead of reaching a plateau after T_C further strongly increases, reaching a high value of $R\ln 9$ at RT. In contrast to zero-field behavior, this function taken at 9 T goes smoothly around T_C with lower magnitudes, growing the transition point up to about 130 K.

Finally, in Fig. 8 is depicted the evolution of the magnetic heat capacity C_m of UCu_2Si_2 upon applying an external magnetic field B up to 9 T. The data were taken at temperatures 90–130 K for $B \parallel c$, i.e., along the easy axis. As one could expect, the λ-shaped peak at T_C determined at zero field begins to diminish continuously with increasing magnetic field strength, becoming more and more broadened, as we have also observed in the case of UGe_2.[37] In such a situation, as a signature of the transition point, we took their inflection points T_{inf} 's. As seen from the inset of this figure, T_{inf} shifts towards higher temperatures with growing strength of magnetic field. In this inset, we have also plotted T_{max} of these curves, which changes with increasing field almost linearly. Thus, such a behavior of the magnetic transition point is characteristic of the localized ferromagnetic systems (see, e.g., Refs. 47–49).

D. Thermal conductivity

The thermal conductivity of UCu_2Si_2 has not been reported up to now. In Fig. 9, we show the total thermal conductivity κ_t as a function of temperature T measured with the thermal gradient ΔT parallel to the ab plane. The small thickness of the used crystal has not allowed for such measurements along the c axis. For a measured plane, we observe first a linear T dependence at low temperatures, then with increasing temperature the $\kappa_t(T)$ curve goes through a shallow maximum at T_{max} (≈70 K) which is followed by a small minimum at T_{min} at about 100 K. This means that the temperature dependence of the total conductivity reveals anomalous behavior at T_C of UCu_2Si_2. Above this temperature, $\kappa_t(T)$ starts again to increase linearly, first with a smaller slope up to T_{slop} (≈200 K) and then at higher temperatures with a larger one. On the other hand, such a behavior of $\kappa_t(T)$ is very similar to that observed for an isostructural silicide, namely, for $CeCu_2Si_2$, although the latter silicide is a magnetically nonordered compound. Nevertheless, for this cerium-based Kondo compound, $\kappa_t(T)$ also goes through a maximum at T_{max} (≈50 K) and then at T_{min} (≈100 K).[50] Interestingly, a third-order perturbation calculation of the thermal conductivity performed for this silicide gave good agreement with the experiment.[51] As found for UCu_2Si_2, both the low- and high-temperature regions of

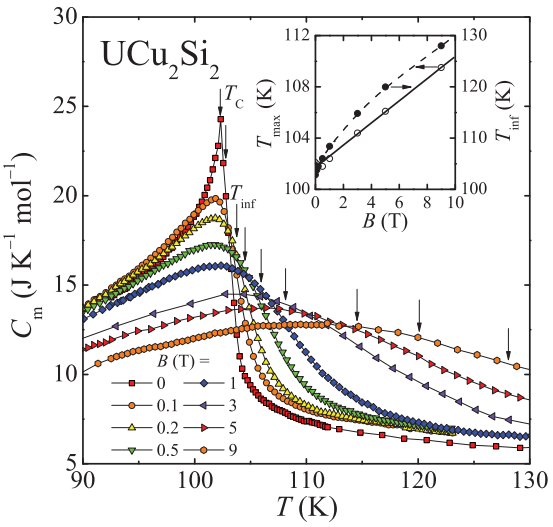

FIG. 8. (Color online) Magnetic heat capacity C_m as a function of temperature measured under applied magnetic fields up to 9 T. Inset: Field dependence of the characteristic temperatures T_C, T_{inf}, and T_{max}.

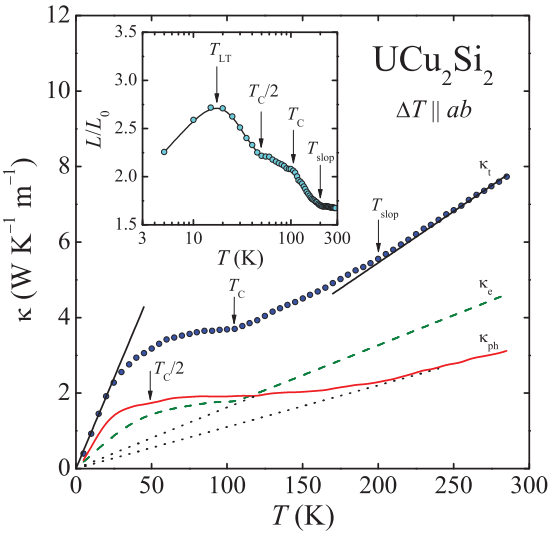

FIG. 9. (Color online) Temperature dependence of thermal conductivity in UCu_2Si_2. Also shown are lattice (κ_{ph}) and electronic (κ_e) components against temperature, assuming $\kappa_e = L_0T/\rho$. In the inset, we plot the L/L_0 ratio vs $\log T$.

$\kappa_t(T)$ for this Ce-based silicide could be approximated also by linear temperature variations. There are also several similar behaviors for other uranium compounds as, for example, in URu_2Si_2 (Ref. 52) and $UCuAs_2$ (Ref. 53). The former compound is well known due to exhibiting at T_0 (=17 K) the so-called hidden order, while the latter is a ferromagnet with $T_C = 131$ K. The onset of the transition at T_0 in URu_2Si_2 is also accompanied with an enhancement in thermal conductivity which leads to its maximum, as is the case of UCu_2Si_2. Although such a maximum (centered at 35 K) is also formed in $UCuAs_2$,[53] its T_{min} is not observed at T_C but at about 40 K below this temperature. The above discussion shows that the magnon contribution into the thermal conductivity situations are different from one compound to another. Since all these mentioned compounds are semimetals with strongly damped free-carrier concentrations, hence, the total thermal conductivity is expected to be significant because of a large contribution of the phonon part κ_{ph}. In addition, owing to the ferromagnetic nature of UCu_2Si_2 and $UCuAs_2$, the magnon contribution κ_m to the $\kappa_t(T)$ dependence should be certainly observed. It originates mainly from the interactions of spin-wave excitations with electrons and phonons. Any separation of this contribution is possible only in the experiment made under applied strong magnetic fields. As shown in Ref. 53, the κ_m contribution in the latter ferromagnet was rather small, amounting to about 10% of the full κ_t magnitude at low temperatures. Therefore, in our analysis we have neglected this contribution, treating it to be less important, and considered only the two most important contributions to κ_t, i.e., the phonon (κ_{ph}) and electronic (κ_e) ones, where $\kappa_t = \kappa_{ph} + \kappa_e$.

One conventional method to separate these two main contributions is supposing the validity of the Wiedemann-Franz (WF) law for the electronic contribution κ_e and using the temperature dependence of the Lorenz number L expressed in Eq. (11):

$$L = \frac{\rho\kappa_e}{T}. \tag{11}$$

According to the WF law in the absence of scattering electrons on phonons, the electronic Lorenz number L becomes for a simple metal equal to the Sommerfeld value $L_0 = 24.4\ \mathrm{nW\,\Omega K^{-2}}$ being independent of temperature. Otherwise, when we have to do with a large contribution of κ_{ph} (see Ref. 50) and then L varies with T as do the main two contributions to κ_t:

$$L(T) = L_0\left(1 + \frac{\kappa_{ph}(T)}{\kappa_e(T)}\right). \tag{12}$$

As the thermal variation of the electrical resistivity of UCu_2Si_2, we have used the data (already published)[13,14] found along the perpendicular direction to the c axis $\rho_\perp(T)$. Its resistivity presents almost temperature-independent behavior in the paramagnetic range and a steep decrease below T_C with a AT^2 law below about 50 K. Finally, one obtains $\kappa_e(T)$ and $\kappa_{ph}(T)$ for this direction taking into account their sum yielding $\kappa_t(T)$, as displayed in Fig. 9. As seen, $\kappa_e(T)$ becomes enhanced with decreasing temperature in the vicinity of T_C while $\kappa_{ph}(T)$ does already in the vicinity of T_{slop}. The latter substantially dominates $\kappa_e(T)$ below T_C, as is the case of URu_2Si_2 below T_0 (see Fig. 4 in Ref. 52). These authors have connected the observed phenomena with a drastic increase in both the phononic and electronic mean-free paths below T_0. Similarly, in UCu_2Si_2, both components considered here decrease their magnitudes below respective T_{max} 's, first slowly and then rapidly but keeping linear behavior when reaching zero at $T = 0$ K. In turn, the inset to Fig. 9 shows a steplike increase below T_{slop} in the L/L_0 ratio plotted against $\log T$. As seen from this inset, the $L(T)/L_0$ function below T_{slop} proceeds by two kinks, in the characteristic temperatures T_C and $T_C/2$, and by a maximum at T_{LT}; all these anomalies correspond to those already described in Sec. III C. Interestingly, this finding confirms well the anomalies observed in the heat-capacity results. Apparently, the thermal conductivity of UCu_2Si_2 is also sensitive to the itinerant part of U-5f electrons in this silicide. The maximum in the L/L_0 ratio is found at about 20 K with a value of 2.75. Then, this ratio decreases gradually to the value being at 5 K only 2.2 larger than the L_0 value, while this ratio at RT is equal to 1.7. In general, all these values are rather small if one compares them to about 16–20 at T_0 found for URu_2Si_2.[52] Moreover, the measurements of the thermal Hall conductivity by the authors of Ref. 54 have pointed out that the observed rapid large increase in both the $\kappa_t(T)$ and $L(T)/L_0$ functions just at T_0 for the case of URu_2Si_2 results due to a considerable domination of the phonon conducting part. This fact makes a distinct difference in the thermal conduction mechanism existing between these two compared here isostructural compounds, differing only in a transition metal, i.e., Cu instead Ru, in their chemical formulas. As seen from Fig. 9, at higher temperatures, but starting at T_C, the electronic part of the UCu_2Si_2 thermal conductivity slightly dominates the phonon one, but below this temperature the situation is reversed and the phononic contribution becomes slightly higher than the electronic one. This implies a rather small rising in the L/L_0 ratio magnitudes with decreasing temperature compared to the huge ones for URu_2Si_2 (given above).

IV. CONCLUSIONS

The main concern of this paper has been a further recognition of the dual character of the 5f electrons (itinerant and localized) on the basis of magnetic (susceptibility) and thermal (heat-capacity and conductivity) bulk measurements performed on a UCu_2Si_2 single crystal. Previous electrical (resistivity and magnetoresistivity) and thermal (thermoelectric power) transport properties performed for this silicide have provided such types of experimental evidences.[13,14] First of all, we found a Kondo-like behavior and the presence of strong magnetic fluctuations in the ferromagnetic state, both giving rise to the above dualism. At present, the magnetic contribution to the heat capacity was obtained by subtracting the data of the nonmagnetic reference system $ThCu_2Si_2$ having the same crystal structure as UCu_2Si_2. This allowed us to separate both the contributions to magnetic heat capacity originating from itinerant and localized behaviors of the 5f electrons. Similarly, the conduction of heat also provides some support of this kind of behavior of these electrons in UCu_2Si_2. From the point of view of the 5f localization, the strong proof is furnished by detailed crystal-field analysis made for this material.

We undertake a trail to determine the CF potential seen by localized $5f$ electrons in UCu_2Si_2 on the ground of the magnetic susceptibility and the heat-capacity measurements. Our approach is justified by satisfactory agreement of the model and experimental results. This is the second [apart from UGe_2 (Ref. 37)] example of such calculations (in this kind of uranium system) in which the whole complexity of the many-electron $5f^2$ states including the J-mixing effects has been taken into account. In both cases, the crystal-field effect has turned out to be relatively strong, comparable with that presented in the literature for some nonmetallic uranium systems. Similarly, the results of the preliminary AOM simulations have indicated to be not so regular as for nonmetallic compounds. These observations point to a crucial role of some specific microscopic CF mechanisms typical of metallic systems, where two of which reveal to be essential ones, namely, the effectively repulsive hybridization and the attractive virtual bond state contributions.

ACKNOWLEDGMENT

We are grateful to Z. Bukowski for growing the single crystal of UCu_2Si_2 and to H. Schilder for developing his computer program towards AOM and the simultaneous fitting of the heat capacity, for making it available, its engagement, and for kind support.

[1] L. Chełmicki, J. Leciejewicz, and A. Zygmunt, J. Phys. Chem. Solids **46**, 529 (1985).
[2] Z. Ban and M. Sikirica, Z. Anorg. Allg. Chem. **356**, 96 (1967).
[3] A. L. Giorgi, A. C. Lawson, J. A. Goldstone, K. J. Volin, and J. D. Jorgensen, J. Appl. Phys. **63**, 3604 (1988).
[4] F. Honda, N. Metoki, T. D. Matsuda, Y. Haga, and Y. Ōnuki, J. Phys.: Condens. Matter **18**, 479 (2006).
[5] K. Hiebl, P. Rogl, C. Horvath, K. Remschnig, and H. Noël, J. Appl. Phys. **67**, 943 (1990).
[6] R. Troć and Z. Bukowski, Phys. Status Solidi B **243**, 290 (2006).
[7] T. D. Matsuda, Y. Haga, S. Ikeda, A. Galatanu, E. Yamamoto, H. Shishido, M. Yamada, J. Yamaura, M. Hedo, Y. Uwatoko *et al.*, J. Phys. Soc. Jpn. **74**, 1552 (2005).
[8] Z. Fisk, N. O. Moreno, and J. D. Thompson, J. Phys.: Condens. Matter **15**, S1917 (2003).
[9] J. A. Morkowski, G. Chełkowska, M. Werwiński, A. Szajek, R. Troć, and C. Neise, J. Alloys Compd. **509**, 6994 (2011).
[10] G. Zwicknagl, A. N. Yaresko, and P. Fulde, Phys. Rev. B **65**, 081103 (2002).
[11] L. M. Sandratskii and J. Kübler, Phys. Rev. B **50**, 9258 (1994).
[12] T. Endstra, G. J. Nieuwenhuys, and J. A. Mydosh, Phys. Rev. B **48**, 9595 (1993).
[13] R. Troć, M. Samsel-Czekała, J. Stępień-Damm, and B. Coqblin, Phys. Rev. B **85**, 224434 (2012).
[14] R. Troć, M. Samsel-Czekała, and B. Coqblin, Acta Phys. Polon. A **121**, 1023 (2012).
[15] K. Hiebl, J. Phys. Soc. Jpn. **67**, 2048 (1998).
[16] Z. Żołnierek and J. Mulak, J. Magn. Magn. Mater. **140–144**, 1393 (1995).
[17] J. A. Mydosh and P. M. Oppeneer, Rev. Mod. Phys. **83**, 1301 (2011).
[18] K. Hanzawa, J. Phys. Soc. Jpn. **81**, 114713 (2012).
[19] E. Ressouche, R. Ballou, F. Bourdarot, D. Aoki, V. Simonet, M. T. Fernandez-Diaz, A. Stunault, and J. Flouquet, Phys. Rev. Lett. **109**, 067202 (2012).
[20] M. B. Silva Neto, A. H. Castro Neto, D. J. Mixson, J. S. Kim, and G. R. Stewart, Phys. Rev. Lett. **91**, 257206 (2003).
[21] B. Coqblin, J. R. Iglesias, N. B. Perkins, A. S. da R. Simoes, and C. Thomas, Phys. B (Amsterdam) **404**, 2961 (2009), and references therein.
[22] T. D. Matsuda, S. Ikeda, E. Yamamoto, Y. Haga, H. Shishido, H. Yamagami, R. Settai, and Y. Ōnuki, J. Phys. Soc. Jpn. **79**, 114712 (2010).
[23] S. F. Matar, V. Siruguri, and V. Eyert, J. Magn. Magn. Mater. **305**, 264 (2006).
[24] H. Takahashi and T. Kasuya, J. Phys. C: Solid State Phys. **18**, 2697 (1985).
[25] B. R. Cooper, R. Siemann, D. Yang, P. Thayamballi, and A. Banerjea, in *Handbook on the Physics and Chemistry of the Actinides*, edited by A. J. Freeman and G. H. Lander, Vol. 2 (Elsevier, Amsterdam, 1985), p. 435.
[26] P. Santini and G. Amoretti, Phys. Rev. Lett. **73**, 1027 (1994).
[27] P. Santini, Phys. Rev. B **57**, 5191 (1998).
[28] H. Amitsuka and T. Sakakibara, J. Phys. Soc. Jpn. **63**, 736 (1994).
[29] A. Galatanu, Y. Haga, T. D. Matsuda, S. Ikeda, E. Yamamoto, D. Aoki, T. Takeuchi, and Y. Ōnuki, J. Phys. Soc. Jpn. **74**, 1582 (2005).
[30] G. Neumann, J. Langen, H. Zahel, D. Plümacher, Z. Kletowski, W. Schlabitz, and D. Wohlleben, Z. Phys. B **59**, 133 (1985).
[31] A. Iandelli and A. Palenzona, in *Handbook of the Physics and Chemistry of Rare Earths*, edited by K. A. Gsschneidner and L. Eyring, Vol. 2 (North Holland, Amsterdam, 1979), p. 1.
[32] R. D. Shannon, Acta Crystallogr. A **32**, 751 (1976).
[33] B. G. Wybourne, *Spectroscopic Properties of Rare Earths* (Wiley, New York, 1965).
[34] K. W. H. Stevens, Proc. Phys. Soc. Sec. A **65**, 209 (1952).
[35] Z. Gajek, J. Phys.: Condens. Matter **12**, 415 (2000).
[36] Z. Gajek, J. C. Krupa, and E. Antic-Fidancev, J. Phys.: Condens. Matter **9**, 557 (1997).
[37] R. Troć, Z. Gajek, and A. Pikul, Phys. Rev. B **86**, 224403 (2012).
[38] Z. Gajek, Phys. Rev. B **72**, 045139 (2005).
[39] The program CONDON is free software, covered by the GNU General Public License, and is available from http://www.condon.fh-aachen.de
[40] H. Schilder (private communication).
[41] J. Mulak and Z. Gajek, *The Effective Crystal Field Potential* (Elsevier, Amsterdam, 2000).
[42] P. Svoboda, P. Javorský, M. Diviš, V. Sechovský, F. Honda, G. Oomi, and A. A. Menovsky, Phys. Rev. B **63**, 212408 (2001).
[43] A. L. Cornelius, J. S. Schilling, T. Endstra, and J. A. Mydosh, AIP Conf. Proc. **309**, 1457 (1994).
[44] B. Renker, F. Gompf, E. Gering, P. Frings, H. Rietschel, R. Felten, F. Steglich, and G. Weber, Phys. B (Amsterdam) **148**, 41 (1987).
[45] K. Schotte and U. Schotte, Phys. Lett. A **55**, 38 (1975).

[46]H.-U. Desgranges and K. D. Schotte, Phys. Lett. A **91**, 240 (1982).
[47]T. Plackowski and D. Kaczorowski, Phys. Rev. B **72**, 224407 (2005).
[48]A. P. Pikul, D. Kaczorowski, H. Michor, P. Rogl, E. Bauer, G. Hilscher, and Y. Grin, J. Phys.: Condens. Matter **15**, 8837 (2003).
[49]E. Colineau, F. Wastin, J. P. Sanchez, and J. Rebizant, J. Phys.: Condens. Matter **20**, 075207 (2008).
[50]W. Franz, A. Griessel, F. Steglich, and D. Wohlleben, Z. Phys. B **31**, 7 (1978).
[51]C. Ayache, M. Raki, B. Salce, D. Schmitt, A. K. Bhattacharjee, and B. Coqblin, J. Phys. Colloques (Paris) **49**, C8-791 (1988).
[52]K. Behnia, R. Bel, Y. Kasahara, Y. Nakajima, H. Jin, H. Aubin, K. Izawa, Y. Matsuda, J. Flouquet, Y. Haga*et al*., Phys. Rev. Lett. **94**, 156405 (2005).
[53]J. Mucha, H. Misiorek, D. Kaczorowski, and A. Jeżowski, J. Alloys Compd. **189**, 217 (1992).
[54]P. A. Sharma, N. Harrison, M. Jaime, Y. S. Oh, K. H. Kim, C. D. Batista, H. Amitsuka, and J. A. Mydosh, Phys. Rev. Lett. **97**, 156401 (2006).